remote sensing

MDPI

Article

A Martian Analogues Library (MAL) Applicable for Tianwen-1 MarSCoDe-LIBS Data Interpretation

Changqing Liu, Zhongchen Wu, Xiaohui Fu, Ping Liu, Yanqing Xin, Ayang Xiao, Hongchun Bai, Shangke Tian, Sheng Wan, Yiheng Liu, Enming Ju, Guobin Jin, Xuejin Lu, Xiaobin Qi and Zongcheng Ling *

Shandong Key Laboratory of Optical Astronomy and Solar-Terrestrial Environment, School of Space Science and Physics, Institute of Space Sciences, Shandong University, Weihai 264209, China; liucq@mail.sdu.edu.cn (C.L.); z.c.wu@sdu.edu.cn (Z.W.); fuxh@sdu.edu.cn (X.F.); liu_ping@sdu.edu.cn (P.L.); yqxin@sdu.edu.cn (Y.X.); ayang_xiao@sdu.edu.cn (A.X.); baihc@mail.sdu.edu.cn (H.B.); sktian@mail.sdu.edu.cn (S.T.); planetarywans@mail.sdu.edu.cn (S.W.); liuyiheng@mail.sdu.edu.cn (Y.L.); enmingju@mail.sdu.edu.cn (E.J.); 202017718@mail.sdu.edu.cn (G.J.); luxuejin@mail.sdu.edu.cn (X.L.); xiaobinqi@mail.sdu.edu.cn (X.Q.)

* Correspondence: zcling@sdu.edu.cn

Abstract: China's first Mars exploration mission, named Tianwen-1, landed on Mars on 15 May 2021. The Mars Surface Composition Detector (MarSCoDe) payload onboard the Zhurong rover applied the laser-induced breakdown spectroscopy (LIBS) technique to acquire chemical compositions of Martian rocks and soils. The quantitative interpretation of MarSCoDe-LIBS spectra needs to establish a LIBS spectral database that requires plenty of terrestrial geological standards. In this work, we selected 316 terrestrial standards including igneous rocks, sedimentary rocks, metamorphic rocks, and ores, whose chemical compositions, rock types, and chemical weathering characteristics were comparable to those of Martian materials from previous orbital and in situ detections. These rocks were crushed, ground, and sieved into powders less than <38 μm and pressed into pellets to minimize heterogeneity at the scale of laser spot. The chemical compositions of these standards were independently measured by X-ray fluorescence (XRF). Subsequently, the LIBS spectra of MAL standards were acquired using an established LIBS system at Shandong University (SDU-LIBS). In order to evaluate the performance of these standards in LIBS spectral interpretation, we established multivariate models using partial least squares (PLS) and least absolute shrinkage and selection (LASSO) algorithms to predict the abundance of major elements based on SDU-LIBS spectra. The root mean squared error (RMSE) values of these models are comparable to those of the published models for MarSCoDe, ChemCam, and SuperCam, suggesting these PLS and LASSO models work well. From our research, we can conclude that these 316 MAL targets are good candidates to acquire geochemistry information based on the LIBS technique. These targets could be regarded as geological standards to build a LIBS database using a prototype of MarSCoDe in the near future, which is critical to obtain accurate chemical compositions of Martian rocks and soils based on MarSCoDe-LIBS spectral data.

Keywords: LIBS; Mars; Martian Analogues Library; MarSCoDe; multivariate models

Citation: Liu, C.; Wu, Z.; Fu, X.; Liu, P.; Xin, Y.; Xiao, A.; Bai, H.; Tian, S.; Wan, S.; Liu, Y.; et al. A Martian Analogues Library (MAL) Applicable for Tianwen-1 MarSCoDe-LIBS Data Interpretation. *Remote Sens.* **2022**, *14*, 2937. https://doi.org/10.3390/rs14122937

Academic Editor: Giancarlo Bellucci

Received: 15 April 2022
Accepted: 9 June 2022
Published: 20 June 2022

1. Introduction

Tianwen-1 is China's first Mars exploration mission, which successfully landed in southern Utopia Planitia on the northern hemisphere of Mars on 15 May 2021 [1–4]. The Zhurong rover was released and traveled more than 1000 m in the Late Hesperian-aged geologic unit of Vastitas Boreals Formation (VBF) [1,4–6], which covers most of the northern plains of Mars. The Mars Surface Composition Detector (MarSCoDe) instrument suite onboard the Zhurong rover combines laser-induced breakdown spectroscopy (LIBS), short-wave infrared (SWIR), and micro-imaging (MI) techniques aiming to obtain elemental compositions (Si, Al, Fe, Ca, Mg, K, Na, O, H, etc.), mineralogy and morphology information

of Martian rocks and soils, respectively [7–9]. The in situ surveys of the Zhurong rover at a new landing site would provide critical ground truths of compositions on Martian surface.

LIBS is one technique for elemental analysis using the optical emission lines from a plasma excited by a focused pulsed laser. Quantitative LIBS analyses of geological samples are hampered by their complex chemical matrix effects, i.e., the emission lines of one element in the plasma always interfere with others [10,11]. For example, in NaCl–$CaCl_2$ brines with constant Ca cations but different NaCl concentrations, the intensities of Ca emission lines are different due to the diverse electron temperature (*Te*) and density (*Ne*) in plasma caused by different concentrations of NaCl [11]. An effective approach to overcome the chemical matrix effects involves using multivariate statistical methods built using a large number of calibration standards, which has been successfully applied to other LIBS payloads such as ChemCam onboard the Curiosity rover [12–14] and SuperCam onboard the Perseverance rover [15]. Thus, calibration standards are the keys to multivariate analysis of LIBS spectra acquired by MarSCoDe with the intent to obtain reliable chemical information.

Based on previous studies by ChemCam, there are several rules for selecting calibration standards:

(1) The number of standards should be sufficient. The ChemCam team originally selected 66 standards [12] and then a much larger set of standards with 408 samples [13] was replenished to build preciser models to interpret ChemCam spectra with complex elemental compositions and mineral diversity at the Gale crater [13,16] (e.g., the RMSE of SiO_2 reduced from 7.1 wt.% to 5.3 wt.%). Dyar et al. (2021) also found that a larger number of training standards could obtain higher prediction accuracy [17].

(2) The calibration standards should cover the diversity of martian rocks and contain a wide concentration of all major elemental compositions (K, Na, Ca, Mg, Al, Fe, Si, etc.). For example, the targets with high-Fe abundances were underestimated at the Vera Rubin Ridge of the Gale crater due to the low fraction of high-Fe samples in 408 standards [18]. David et al. (2021) extended the concentration of FeOT using iron oxide mixed with the Martian regolith simulant (JSC-1), and better results were obtained for samples with FeOT > 80 wt.% (RMSE = ~7 wt.%).

(3) The standards should be representative of typical minerals and rocks on Mars, including primary (e.g., basalt, andesite, pyroxene, feldspar, olivine, etc.) and secondary minerals and rocks (clays, sulfates, chloride, etc.) [19]. For example, some targets in the ChemCam standards library were excluded due to their significant difference from most Martian rocks [13]. These targets contain different emission behaviors from typical Martian materials, and thus influence the prediction accuracy.

Based on these considerations, 316 terrestrial rocks were selected to establish one Martian Analogues Library (MAL) as the calibration sample set for MarSCoDe-LIBS data. With the intent to verify the availability of MAL targets in LIBS spectral investigations, we built a LIBS spectral database using a LIBS system at Shandong University (SDU-LIBS), and subsequently, 100 multivariate models were built using partial least squares (PLS) and least absolute shrinkage and selection (LASSO) algorithms. The MAL standards in our work will be used to build a LIBS database using MarSCoDe-P (MarSCoDe prototype, a copy of MarSCoDe payload onboard the Zhurong rover) in the future, which is critical to LIBS spectral interpretation and elemental quantification obtained by MarSCoDe on Mars.

2. Methods

2.1. Samples for MAL

The MAL includes 316 pressed powder samples. We selected 316 terrestrial rocks and minerals according to the rules mentioned above, including 188 igneous rocks, 58 sedimentary rocks, 56 metamorphic rocks, as well as 14 ores. These samples were crushed, ground, and sieved (using a sieve of 400 mesh) to acquire grains smaller than 38 μm (Figure 1), with the intent to guarantee the homogeneity of these standards at the LIBS beam scale of MarSCoDe (110–180 μm at the distance of 3–5 m [7]). Finally, 27.74 kg powder samples were obtained (Figure 2), including 16.3 kg igneous samples, 5.5 kg sedimentary

samples, 4.3 kg metamorphic samples, and 1.7 kg ores. In this work, the powder standards in MAL were pressed to pellet at ~200 MPa for 2 min. The pellet was 2 cm in diameter with a protective surrounding of boric acid (Figure 1).

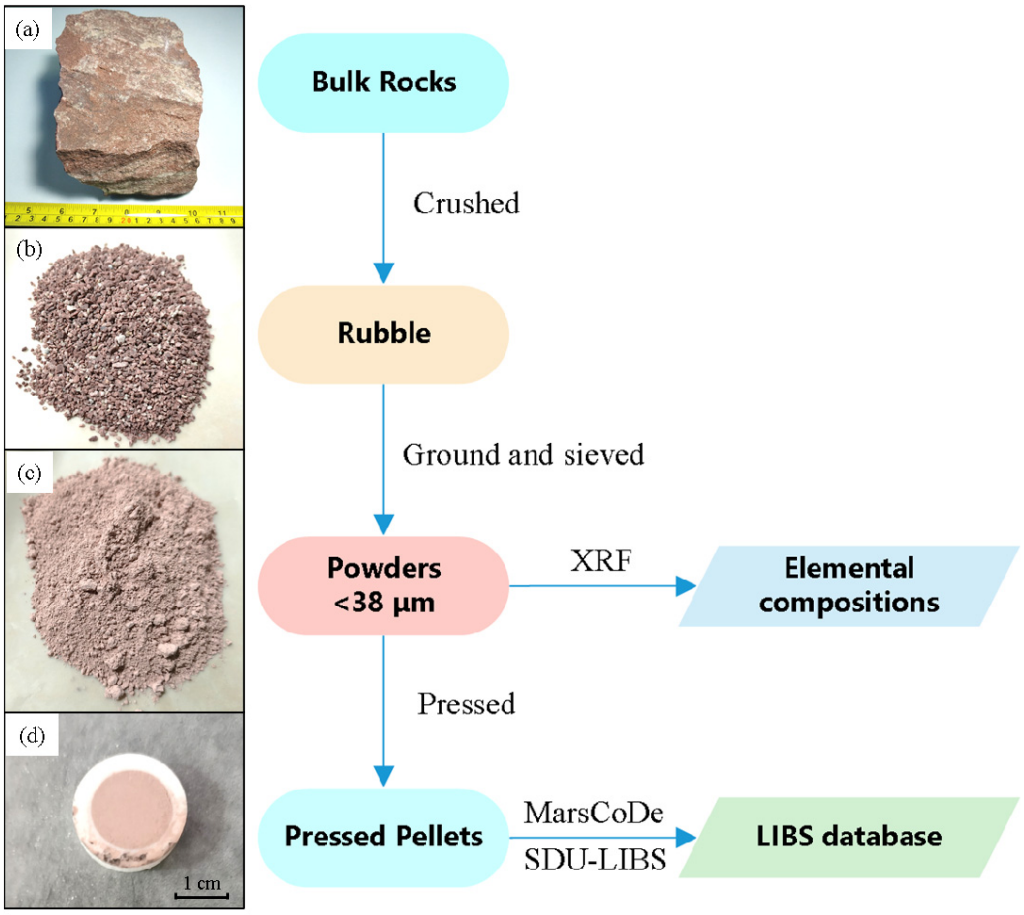

Figure 1. Scheme for MAL standards preparation and images of feldspathic quartz sandstone (SDU-001-SEC): (**a**) Original rock; (**b**) fragments; (**c**) powders < 38 μm; (**d**) pellet.

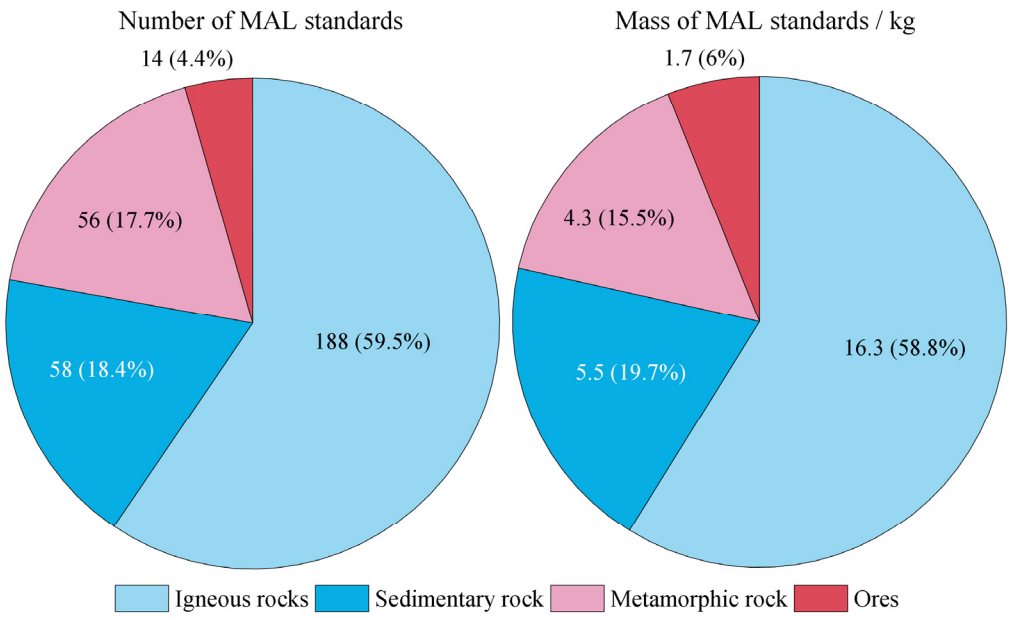

Figure 2. Pie graph of number and mass (kg) of MAL standards.

The elemental compositions of these powders were measured using ARL Perfom'X 4200 X-ray fluorescence (XRF) spectrometry at the State Key Laboratory of ORE Deposit Geochemistry, Chinese Academy of Sciences. The errors of major elements were confirmed using twelve published standards including GBW03131, GBW07821, GBW03130, GBW03134, GBW07123, GSR-1-5, GSR-7, and GSR-18, which were 0.35 wt.% for SiO_2, 0.13 wt.% for Al_2O_3, 0.12 wt.% for Fe_2O_3T, 0.11 wt.% for MgO, 0.11 wt.% for CaO, 0.10 wt.% for Na_2O, 0.02 wt.% for K_2O, and 0.34 wt.% for TiO_2.

2.2. LIBS Instrument and Experimental Layout

The SDU-LIBS system is described in detail in Liu et al. [20]. Briefly, it utilizes an Nd:YAG laser to produce 8 ns pulses of 1064 nm laser beam with an energy of 200 mJ. The laser beam is expanded and focused on targets through a 120 mm diameter Schmidt–Cassegrain telescope. Targets are ablated by the focused laser (~4 GW/cm^2 on targets). The optical emissions from the excited plasma are collected by the same telescope, divided into three beams by a demultiplexer, and then transferred into three spectrometers. The LIBS system can collect LIBS spectra in 250–850 nm, except 339–354 nm and 549–570 nm regions. In this work, the LIBS spectra of pressed pellets were collected from three different points, and emissions from ten excited plasmas were averaged at each point. The experiment was performed in a Mars-like atmosphere (7 mbar CO_2) in a Mars Environment Chamber [21].

2.3. LIBS Spectral Processing

The SDU-LIBS spectra used in this study were preprocessed as described in [20] to remove instrument white noise and continuum spectra using the Daubechies Wavelet function and interpolated spline function, respectively. Subsequently, each spectrum was normalized using the maximum intensity of emission lines, resulting in a spectrum within 0–1, which would mitigate fluctuations in LIBS signal between different samples. The commonly used normalization methods were not used in this study including normalization using the full spectrum of three spectrometers (Norm 1) and normalization on a per-spectrometer basis (Norm 3) [12–14] due to the significant effects of the elements with several emission lines (e.g., Fe). An example of the LIBS spectrum from feldspathic quartz sandstone (SDU-001-SEC) is exhibited in Figure 3. LIBS emission lines of eleven elements (Si, Fe, Mg, K, Na, Ti, Ca, Al, O, H, and C) were identified based on the NIST database [22]. It should be noticed that H and C emission lines may also be contributed by the surrounding atmosphere.

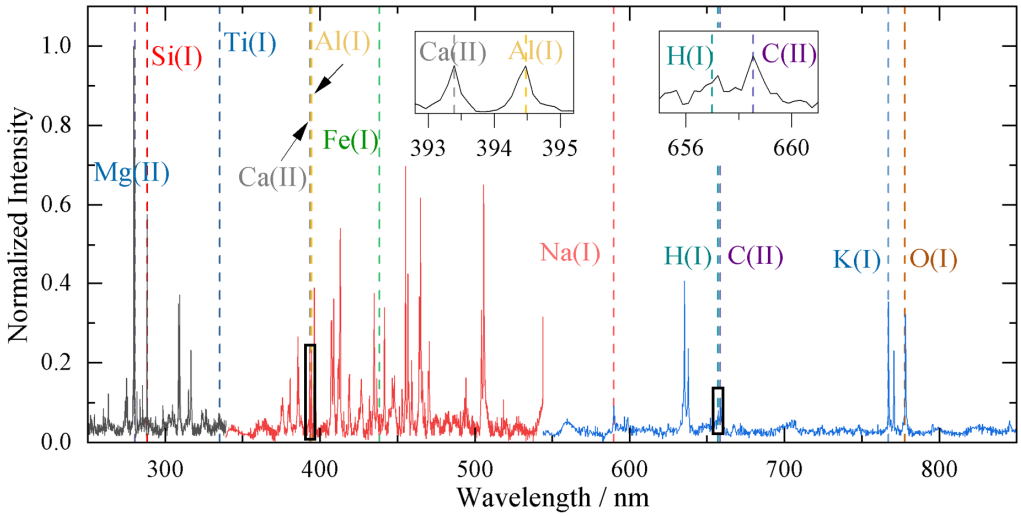

Figure 3. Example of a LIBS spectrum from feldspathic quartz sandstone (SDU-001-SEC). The emission lines of eleven elements (Si, Fe, Mg, K, Na, Ti, Ca, Al, O, H, and C) were identified based on the NIST database [22]. The black, red, and blue segments are corresponding to the three spectral channels.

2.4. Multivariate Models

PLS and LASSO are commonly used multivariate regression methods to interpret spectroscopic spectra of geological samples [15,23–26]. We built 100 multivariate models using PLS and LASSO algorithms as follows:

(1) Dividing training set and test set. We randomly divided the LIBS spectra of a full set of MAL standards into a training set and a test set at the approximate ratio of 1:4, which means that LIBS spectra of random 252 samples were selected as a training set to build models, and spectra from the other 64 samples were a test set for model verification using root mean squared error (RMSE).
(2) Hyperparameter optimization. The number of latent variables (H) of PLS was initially set as 1–50, and alpha values in LASSO were originally set as 0.02–1.0. The H and alpha values were iteratively optimized based on their RMSE values in specified maximum iteration times of 2000. In all cases, H and alpha values were in the range of 3–29 (average 13) and 0.02–0.1 (average 0.036), respectively.
(3) Iteration. The processes above were repeated 50 times to verify the robustness of these models. 50 PLS and 50 LASSO models were finally established.

3. Results and Discussion

3.1. Elemental Compositions of MAL

The oxides of eight major elements of all MAL standards are exhibited in Figure 4 and compared to the 408 standards for ChemCam (a widely-used LIBS standard library) [13]. The distribution of compositions of MAL standards is similar and comparable to the ChemCam standards, suggesting a reasonable composition distribution of MAL standards.

In terms of major elements (Si, Fe, Al, Ti, etc.), the oxides of major elements in MAL standards are 0–99.9 wt.% for SiO_2, 0–44.7 wt.% for TiO_2, 0–62.4 wt.% for Al_2O_3, 0–85.5 wt.% for Fe_2O_3T, 0–47.6 wt.% for MgO, 0.1–70.6 wt.% for CaO, 0–22.4 wt.% for Na_2O, and 0–14.9 wt.% for K_2O, respectively. MAL has 278 silicate standards with the SiO_2 concentration from 12.5 wt.% (breccia) to 99.9 wt.% (quartz), including igneous rocks (e.g., basalt), metamorphic rocks (e.g., serpentinite), clastic sediments (e.g., feldspathic quartz sandstone shown in Figure 1), and silica-rich minerals (e.g., olivine, pyroxene, kaolinite, montmorillonite, etc.). Several ores are also included with the high abundance of Fe_2O_3T (up to 79.8 wt.% from hematite), Al_2O_3 (up to 62.4 wt.% from spinel), and TiO_2 (up to 44.7 wt.% from ilmenite).

MAL also contains some standards with high concentrations of minor and trace elements. Ten sulfates (e.g., Ca-sulfate) and nine sulfides (e.g., pyrrhotite) are included with S concentrations of 0.5–27.3 wt.%, while a blend (ZnS, SDU-291-ORE) has a low concentration of S (0.5 wt.%) but a high abundance of SiO_2 (88.2 wt.%), which may be affected by surrounding quartz. A fluorite with a F concentration of 39.0 wt.% is also included in MAL. A silicate mineral sodalite (SDU-077-IGN) contains Cl of 6.4 wt.%. MAL also contains other elements of P_2O_5 (0–2.4 wt.%), As (0–0.7 wt.%), Ba (0–57.3 wt.%), Cu (0–27.7 wt.%), Sr (0–1.3 wt.%), Zn (0–51.2 wt.%), Zr (0–2.8 wt.%), W (0–1.1 wt.%), Sn (0–3.1 wt.%), Pb (0–59.8 wt.%), and Mn (0–17.2 wt.%). In terms of carbonate, MAL also contains twelve carbonate-rich targets including marble, calcite, limestone, and dolomite, but the abundance of C is not provided by XRF measurements.

Overall, the concentrations of major, minor, and trace elements in MAL standards are obtained including Si, Fe, Mg, K, Na, Ti, Ca, Al, S, F, Cl, P, As, Ba, Cu, Sr, Zn, Zr, W, Sn, Pb, and Mn. The abundance of these elements can be used to build models to derive compositions of unknown targets.

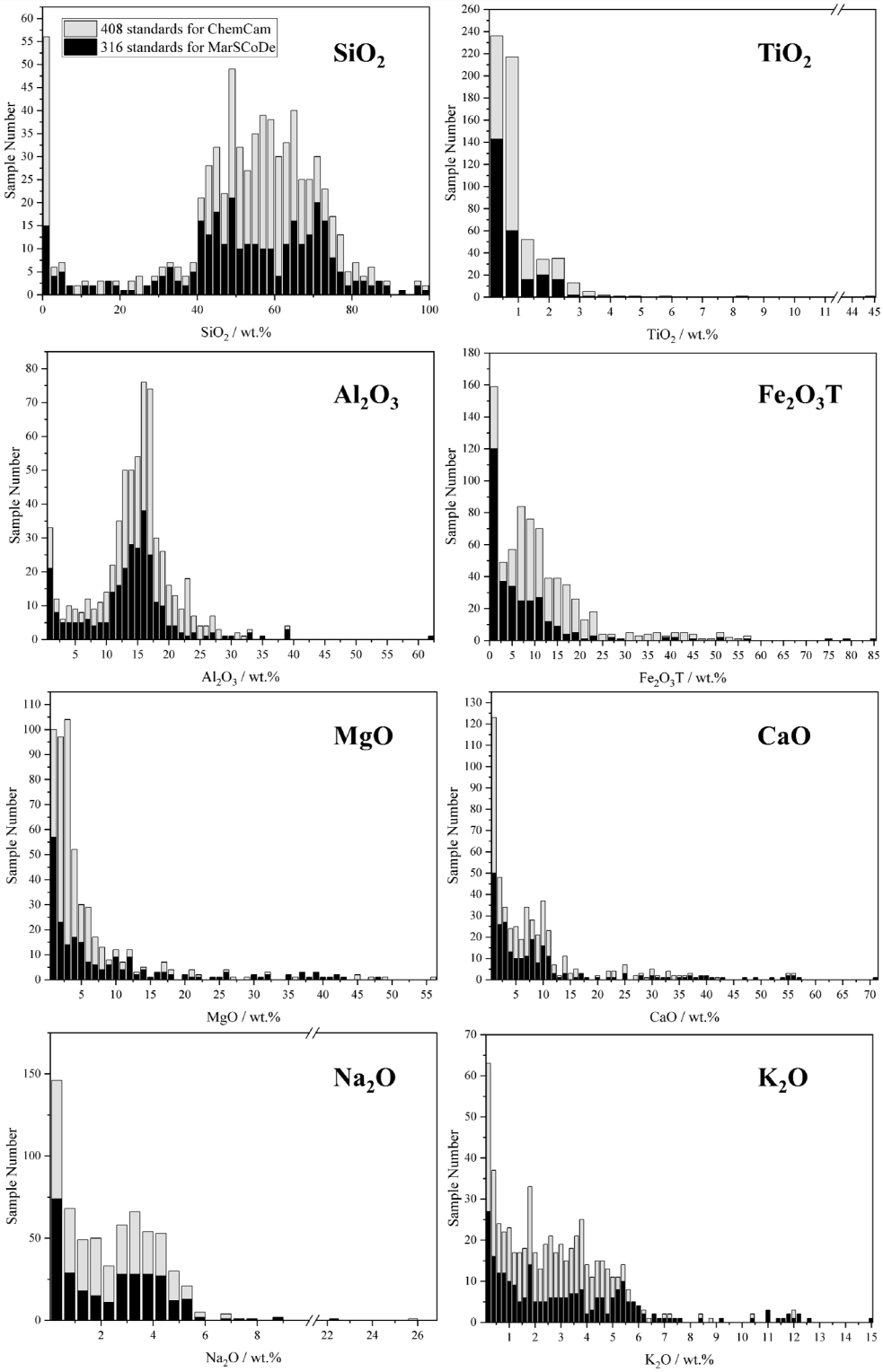

Figure 4. The distribution of oxides of major elements in 408 standards for ChemCam (gray) and 316 standards for MarSCoDe.

3.2. Geochemical Characteristics of MAL

The geochemical characteristics of MAL standards are demonstrated using a total alkali-silica (TAS) diagram and ternary diagrams of Al_2O_3-(CaO + Na_2O)-K_2O and Al_2O_3-(CaO + Na_2O + K_2O)-(FeO_T + MgO) (Figure 5), which are widely-used methods to characterize geochemistry and the evolution of igneous and sedimentary rocks. On a TAS diagram (Figure 5a), most MAL standards are distributed and filled the region of typical igneous

rocks including tephrite, basalt, andesite, dacite, trachyte, phonolite, etc. These targets are uniformly distributed along the alkaline-subalkaline boundary, from Irvine et al. (1971) and Sautter et al. (2015) [27,28]. Moreover, a high density of standards is observed near the typical compositions of Martian soils and rocks including TES-derived data, GRS results, and the in situ detections at the Pathfinder landing site, Gusev crater, and Meridiani Planum [29]. The distribution of these targets suggests that the MAL standards are representative of Martian igneous materials.

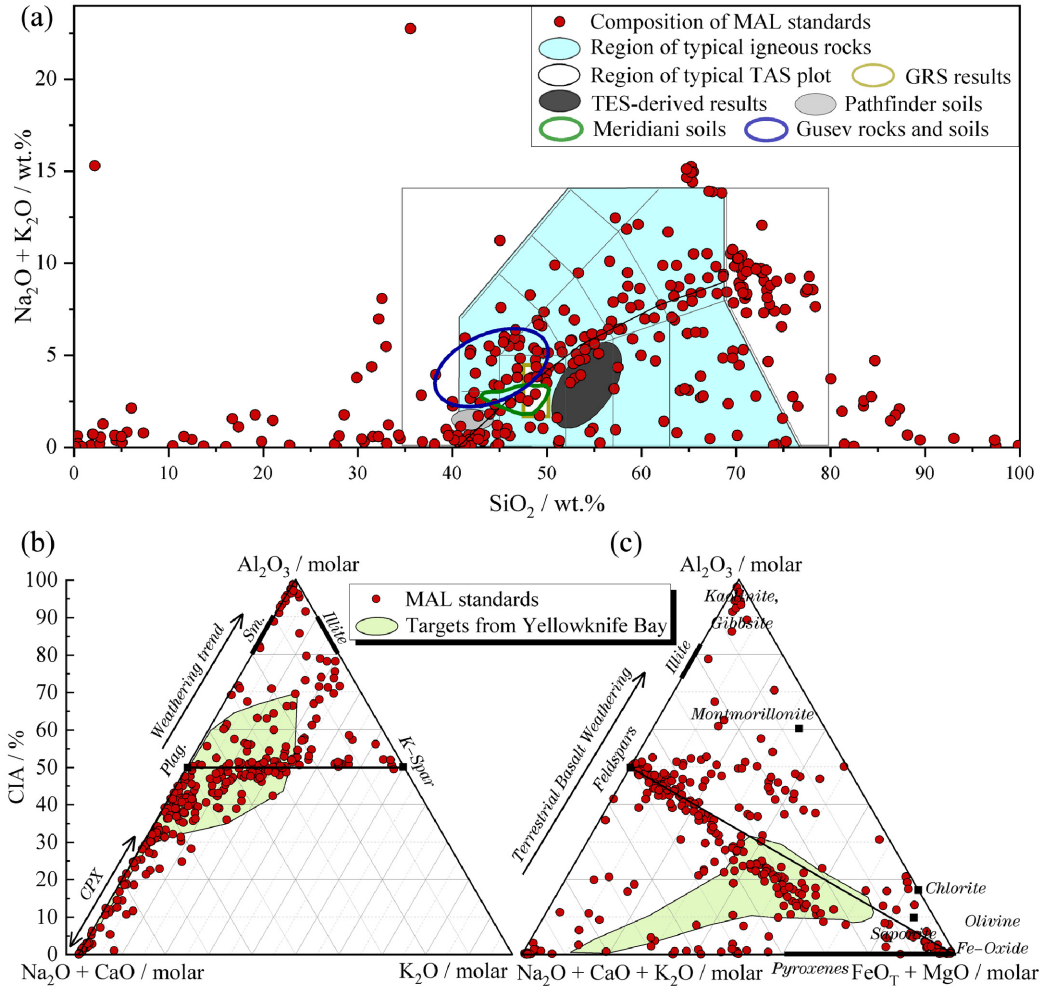

Figure 5. Geochemical characteristics of MAL standards: (**a**) Total alkali-silica plot of all 316 MAL standards, with the TES-derived data and GRS results, as well as compositions of rocks and soils at the Pathfinder landing site, Gusev crater, and Meridiani Planum from McSween et al. (2009) [29]. The polyline in the region of typical igneous rocks (cyan) is the alkaline–subalkaline boundary from Irvine et al. (1971) and Sautter et al. (2015) [27,28]; (**b**) ternary diagram of Al_2O_3-(CaO + Na_2O)-K_2O with CIA values on the vertical axis; (**c**) ternary diagram of Al_2O_3-(CaO + Na_2O + K_2O)-(FeO_T + MgO). ChemCam results from Yellowknife Bay in the Gale crater (green polygon) are from McLennan et al. (2014) [30].

Compositions of MAL standards are compared to the ChemCam results of igneous and secondary targets from Yellowknife Bay in the Gale crater (the green region in Figure 5b,c), which contains most types of Martian rock (e.g., Ca-sulfate, feldspathic targets, mafic targets, clay, etc.) [30]. The ternary diagram of Al_2O_3-(CaO + Na_2O)-K_2O with the chemical index of alteration (CIA) (Figure 5b) provides critical information on chemical weathering [30,31]. Igneous materials lie on or below the line of plagioclase-K-feldspar, and secondary materials with a higher degree of alteration plot above. In the ternary diagram of Al_2O_3-(CaO + Na_2O

+ K_2O)-(FeO_T + MgO) (Figure 5c), most igneous rocks are distributed along a bisecting line of the FeOT + MgO corner, while sedimentary materials with a higher degree of chemical weathering are typically above the line, and most metamorphic rocks are scattered below. The Ca-sulfate-rich targets in the Gale crater are also distributed below the line [30]. Most MAL targets are concentrated in the region of bisecting line, while others are distributed uniformly above and below the line, suggesting the MAL contains the most possible geological types of Martian materials. As compared with the targets at Yellowknife Bay, the MAL standards have more extended compositions of Al_2O_3 (e.g., montmorillonite) and K-rich igneous materials (e.g., K-feldspar), and contain more types of geological materials (e.g., kaolinite).

Overall, the MAL standards contain the most possible types of Martian geological materials including igneous, sedimentary, and metamorphic rocks. The lithology and chemical weathering of these targets are distributed uniformed in the diagrams above. Additionally, these targets have more extended compositions than the Yellowknife Bay materials that contain diverse rock types and a wide composition range, suggesting the MAL standards are representative of Martian materials.

3.3. Multivariate Models for Major Elements

In this work, 50 PLS and 50 LASSO models were established through 50 iterations. The RMSEs of these models are exhibited in Figure 6. The average and standard deviation of 50 RMSEs for each major element are shown in Table 1. The RMSEs of both PLS and LASSO models have small standard deviations (<1.4 wt.%) for SiO_2, Al_2O_3, Fe_2O_3T, CaO, MgO, K_2O, and Na_2O, suggesting low variation of RMSEs, and thus high stability of these models has been achieved. The RMSEs of TiO_2 have higher standard deviations (1.3 wt.% for PLS models and 1.8 wt.% for LASSO models) than other elements, which may be caused by its lower concentration (Figure 4), and thus low intensities of Ti emission lines.

Table 1. The average RMSE (wt.%) of the 50 PLS and 50 LASSO models, and RMSEs of published models for MarSCoDe, ChemCam, and SuperCam.

Models		SiO_2	Al_2O_3	Fe_2O_3T *	TiO_2	CaO	MgO	K_2O	Na_2O
Models in this work	PLS	8.3 ± 1.0	4.2 ± 1.4	4.2 ± 0.7	1.3 ± 1.3	3.2 ± 0.5	3.3 ± 0.4	1.3 ± 0.3	1.1 ± 0.2
	LASSO	9.4 ± 1.2	4.4 ± 1.3	4.8 ± 0.9	1.6 ± 1.8	4.1 ± 0.8	3.7 ± 0.5	1.5 ± 0.3	1.3 ± 0.4
MarSCoDe Performance test [7]		6.9	2.3	- **	-	2.0	-	0.6	0.9
Model for ChemCam [13]		5.3	3.5	2.3 **	1.0	2.7	2.2	0.8	0.6
Model for SuperCam [15]		6.1	1.8	3.1 **	0.3	1.3	1.1	0.6	0.5

* Fe_2O_3T refers to total iron, including both ferric and ferrous. ** The derived Fe from models for MarSCoDe, ChemCam, and SuperCam are given as FeOT.

In addition, the RMSEs of the PLS and LASSO models are comparable to the published models for MarSCoDe [7], ChemCam [13], and SuperCam [15], while all PLS models have lower RMSEs than the LASSO models (Figure 6). For example, the RMSEs of SiO_2 are 8.3 wt.% for the PLS model (this work), 9.4 wt.% for the LASSO model (this work), 6.9 wt.% for the MarSCoDe test model, 5.3 wt.% for the ChemCam model, and 6.1 wt.% for the SuperCam model. The higher RMSEs of the PLS and LASSO models in this work may be mainly due to the lower intensities of SDU-LIBS emission lines but higher noise signals (~80 DN in [20]) of the SDU-LIBS system.

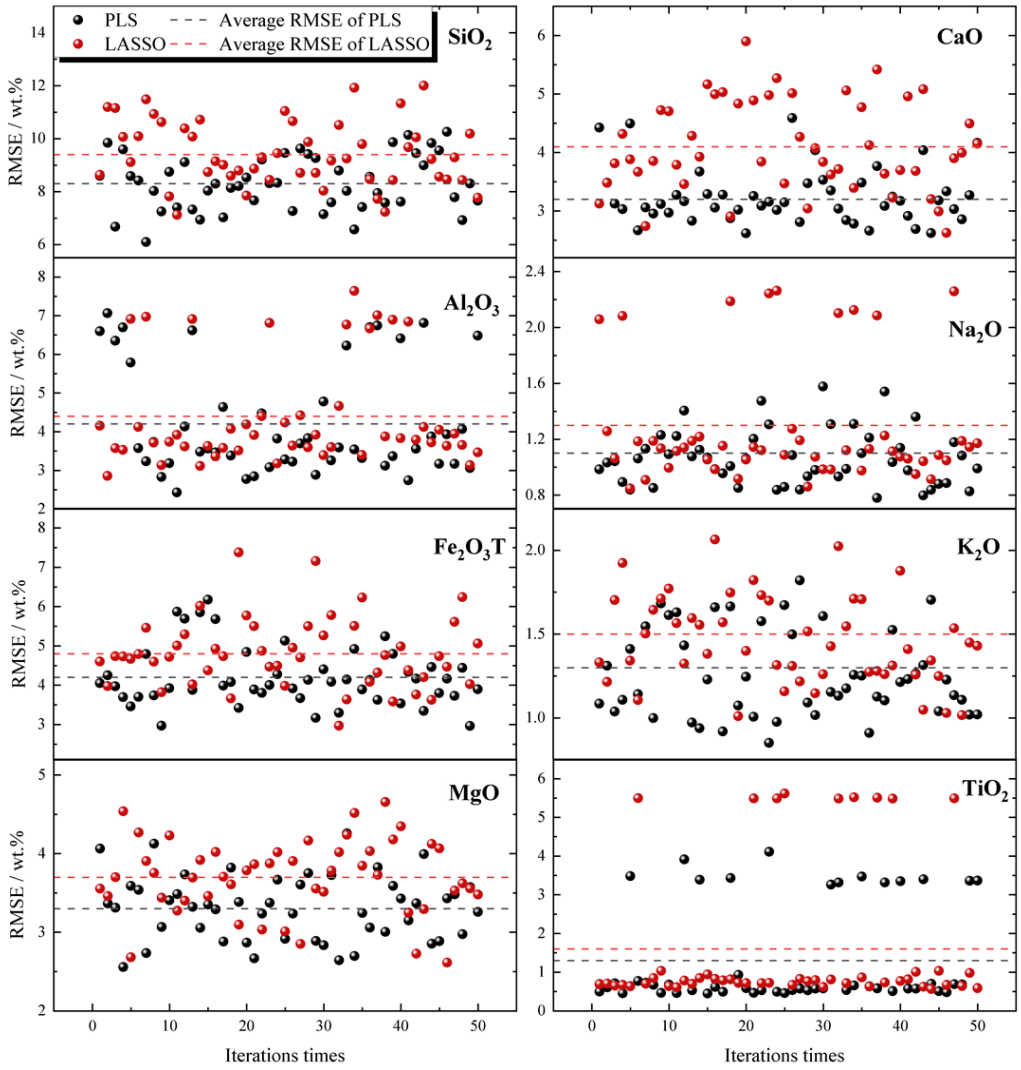

Figure 6. RMSEs of test sets in 50 PLS and 50 LASSO models. Dash lines indicate the average RMSE of 50 RLS models (black line) and 50 LASSO models (red line).

Overall, it can be suggested that the PLS and LASSO models work well, although the models have higher RMSEs than those of the published models for MarSCoDe, ChemCam, and SuperCam. Thus, the MAL standards are applicable to establish models and quantitatively interpret LIBS spectra of unknown targets.

4. Conclusions

Calibration standards are critical to MarSCoDe-LIBS spectral interpretation according to the experience of ChemCam [12,13,16]. In this work, we established a calibration standard library (i.e., MAL) with certain chemical compositions, with the intent to build a LIBS database and models using MarSCoDe-P to interpret MarSCoDe-LIBS spectra on Mars, which would provide reliable chemical compositions of Martian rocks and soils. The MAL contains 316 standards with grains <38 μm, which are developed from 316 terrestrial rocks. The MAL standards contain the most possible types of Martian materials, and their chemical compositions are equably distributed according to lithology and chemical weathering characteristics, indicating their high representation of Martian materials.

The availability of these MAL standards for MarSCoDe-LIBS spectral interpretation was verified by multivariate models based on their SDU-LIBS spectra acquired in simulated Martian environments. Several PLS and LASSO models were developed, and their RMSEs are comparable to those of the published models, suggesting that these models work well

and are applicable to deriving chemical compositions of unknown materials. It should be noted that the MAL standards exhibit different physical states as compared with complex Martian rocks and soils, including grain size, hardness, roughness, absorptivity, thermal conductivity, and degree of crystallinity. Their different physical matrix effects lead to different behaviors of the laser energy coupling with the surface, and thus influence the reliability of models based on MAL powder standards [32–35]. It should be carefully evaluated how the physical matrix effects would affect the accuracy of models built based on MAL standards when deriving chemical compositions of Martian soils and rocks.

From our research, we can conclude that these 316 MAL targets are good candidates to acquire geochemistry information based on LIBS technique. Thus, it can be proposed that MAL standards are applicable for MarSCoDe. More standards will be included according to the compositions and rock types detected by the Zhurong rover. These targets could be regarded as geological standards to build a LIBS database using a prototype of MarSCoDe in the near future, which is critical to obtain accurate chemical compositions of Martian rocks and soils based on MarSCoDe-LIBS spectral data.

Author Contributions: Conceptualization, Z.L.; Data curation, C.L., Y.X., A.X., H.B., S.T., S.W., Y.L., E.J., G.J., X.L. and X.Q.; Formal analysis, C.L.; Funding acquisition, Z.L.; Investigation, C.L.; Methodology, C.L.; Project administration, Z.L.; Resources, Z.L.; Software, C.L.; Supervision, Z.L.; Validation, Z.W., X.F., P.L. and Z.L.; Visualization, C.L.; Writing—original draft, C.L.; Writing—review and editing, C.L., Z.W., X.F., P.L., Y.X., A.X., H.B., S.T., S.W., Y.L., E.J., G.J., X.L., X.Q. and Z.L. This is the SDU-CPS publication #97. All authors have read and agreed to the published version of the manuscript.

Funding: We thank the fundings from the National Natural Science Foundation (U1931211, 11941001, and 41972322) and the Natural Science Foundation of Shandong Province (ZR2019MD008). This research is also funded by the Pre-Research Project on Civil Aerospace Technologies No. D020102 funded by the China National Space Administration (CNSA), and Strategic Priority Research Program, Chinese Academy of Sciences (grant No. XDB41000000).

Data Availability Statement: Please contact the corresponding author.

Conflicts of Interest: The authors declare no conflict of interest.

References

1. Zhao, J.; Xiao, Z.; Huang, J.; Head, J.W.; Wang, J.; Shi, Y.; Wu, B.; Wang, L. Geological characteristics and targets of high scientific interest in the Zhurong landing region on Mars. *Geophys. Res. Lett.* **2021**, *48*, e2021GL094903. [CrossRef]
2. Wu, B.; Dong, J.; Wang, Y.; Li, Z.; Chen, Z.; Liu, W.C.; Zhu, J.; Chen, L.; Li, Y.; Rao, W. Characterization of the Candidate Landing Region for Tianwen-1–China's First Mission to Mars. *Earth Space Sci. Rev.* **2021**, *8*, e2021EA001670. [CrossRef]
3. Wu, X.; Liu, Y.; Zhang, C.; Wu, Y.; Zhang, F.; Du, J.; Liu, Z.; Xing, Y.; Xu, R.; He, Z. Geological characteristics of China's Tianwen-1 landing site at Utopia Planitia, Mars. *Icarus* **2021**, *370*, 114657. [CrossRef]
4. Ye, B.; Qian, Y.; Xiao, L.; Michalski, J.R.; Li, Y.; Wu, B.; Qiao, L. Geomorphologic exploration targets at the Zhurong landing site in the southern Utopia Planitia of Mars. *Earth Planet. Sci. Lett.* **2021**, *576*, 117199.
5. Tanaka, K.L.; Robbins, S.; Fortezzo, C.; Skinner, J., Jr.; Hare, T.M. The digital global geologic map of Mars: Chronostratigraphic ages, topographic and crater morphologic characteristics, and updated resurfacing history. *Planet. Space Sci.* **2014**, *95*, 11–24. [CrossRef]
6. Kreslavsky, M.A.; Head, J.W. Fate of outflow channel effluents in the northern lowlands of Mars: The Vastitas Borealis Formation as a sublimation residue from frozen ponded bodies of water. *J. Geophys. Res. Planets* **2002**, *107*, 4-1–4-25. [CrossRef]
7. Xu, W.; Liu, X.; Yan, Z.; Li, L.; Zhang, Z.; Kuang, Y.; Jiang, H.; Yu, H.; Yang, F.; Liu, C. The MarSCoDe Instrument Suite on the Mars Rover of China's Tianwen-1 Mission. *Space Sci. Rev.* **2021**, *217*, 64. [CrossRef]
8. Jiang, X.; Yang, B.; Li, S. Overview of China's 2020 Mars mission design and navigation. *Astrodynamics* **2018**, *2*, 1–11. [CrossRef]
9. Zou, Y.; Zhu, Y.; Bai, Y.; Wang, L.; Jia, Y.; Shen, W.; Fan, Y.; Liu, Y.; Wang, C.; Zhang, A. Scientific objectives and payloads of Tianwen-1, China's first Mars exploration mission. *Adv. Space Res.* **2021**, *67*, 812–823. [CrossRef]
10. Eppler, A.S.; Cremers, D.A.; Hickmott, D.D.; Ferris, M.J.; Koskelo, A.C. Matrix effects in the detection of Pb and Ba in soils using laser-induced breakdown spectroscopy. *Appl. Spectrosc.* **1996**, *50*, 1175–1181. [CrossRef]
11. Goueguel, C.; Singh, J.P.; McIntyre, D.L.; Jain, J.; Karamalidis, A.K. Effect of sodium chloride concentration on elemental analysis of brines by laser-induced breakdown spectroscopy (LIBS). *Appl. Spectrosc.* **2014**, *68*, 213–221. [CrossRef] [PubMed]

12. Wiens, R.C.; Maurice, S.; Lasue, J.; Forni, O.; Anderson, R.B.; Clegg, S.; Bender, S.; Blaney, D.; Barraclough, B.L.; Cousin, A.; et al. Pre-flight calibration and initial data processing for the Chem Cam laser-induced breakdown spectroscopy instrument on the Mars Science Laboratory rover. *Spectrochim. Acta Part B At. Spectrosc.* **2013**, *82*, 1–27. [CrossRef]
13. Clegg, S.M.; Wiens, R.C.; Anderson, R.; Forni, O.; Frydenvang, J.; Lasue, J.; Cousin, A.; Payre, V.; Boucher, T.; Dyar, M.D.; et al. Recalibration of the Mars Science Laboratory ChemCam instrument with an expanded geochemical database. *Spectrochim. Acta Part B At. Spectrosc.* **2017**, *129*, 64–85. [CrossRef]
14. Anderson, R.B.; Clegg, S.M.; Frydenvang, J.; Wiens, R.C.; McLennan, S.; Morris, R.V.; Ehlmann, B.; Dyar, M.D. Improved accuracy in quantitative laser-induced breakdown spectroscopy using sub-models. *Spectrochim. Acta Part B-At. Spectrosc.* **2017**, *129*, 49–57. [CrossRef]
15. Anderson, R.B.; Forni, O.; Cousin, A.; Wiens, R.C.; Clegg, S.M.; Frydenvang, J.; Gabriel, T.S.; Ollila, A.; Schröder, S.; Beyssac, O. Post-landing major element quantification using SuperCam laser induced breakdown spectroscopy. *Spectrochim. Acta Part B At. Spectrosc.* **2021**, *188*, 106347. [CrossRef]
16. Maurice, S.; Clegg, S.M.; Wiens, R.C.; Gasnault, O.; Rapin, W.; Forni, O.; Cousin, A.; Sautter, V.; Mangold, N.; Le Deit, L.; et al. ChemCam activities and discoveries during the nominal mission of the Mars Science Laboratory in Gale crater, Mars. *J. Anal. At. Spectrom.* **2016**, *31*, 863–889. [CrossRef]
17. Dyar, M.D.; Ytsma, C.R. Effect of data set size on geochemical quantification accuracy with laser-induced breakdown spectroscopy. *Spectrochim. Acta Part B At. Spectrosc.* **2021**, *177*, 106073. [CrossRef]
18. David, G.; Cousin, A.; Forni, O.; Meslin, P.Y.; Dehouck, E.; Mangold, N.; L'Haridon, J.; Rapin, W.; Gasnault, O.; Johnson, J.R.; et al. Analyses of High-Iron Sedimentary Bedrock and Diagenetic Features Observed with ChemCam at Vera Rubin Ridge, Gale Crater, Mars: Calibration and Characterization. *J. Geophys. Res. Planets* **2020**, *125*. [CrossRef]
19. Ehlmann, B.L.; Edwards, C.S. Mineralogy of the Martian Surface. *Annu. Rev. Earth Planet. Sci.* **2014**, *42*, 291–315. [CrossRef]
20. Liu, C.; Ling, Z.; Zhang, J.; Wu, Z.; Bai, H.; Liu, Y. A Stand-Off Laser-Induced Breakdown Spectroscopy (LIBS) System Applicable for Martian Rocks Studies. *Remote Sens.* **2021**, *13*, 4773. [CrossRef]
21. Wu, Z.; Ling, Z.; Zhang, J.; Fu, X.; Liu, C.; Xin, Y.; Li, B.; Qiao, L. A Mars Environment Chamber Coupled with Multiple In Situ Spectral Sensors for Mars Exploration. *Sensors* **2021**, *21*, 2519. [CrossRef] [PubMed]
22. Kramida, A.; Ralchenko, Y.; Reader, J.; NIST ASD Team. *NIST Atomic Spectra Database*; Version 5.8; National Institute of Standards and Technology (NIST): Gaithersburg, MD, USA, 2021. [CrossRef]
23. Haaland, D.M.; Thomas, E.V. Partial least-squares methods for spectral analyses. 1. Relation to other quantitative calibration methods and the extraction of qualitative information. *Anal. Chem.* **1988**, *60*, 1193–1202. [CrossRef]
24. Wold, S.; Albano, C.; Dunn, W.; Edlund, U.; Esbensen, K.; Geladi, P.; Hellberg, S.; Johansson, E.; Lindberg, W.; Sjöström, M. Multivariate data analysis in chemistry. In *Chemometrics*; Springer: Berlin/Heidelberg, Germany, 1984; pp. 17–95.
25. Andries, E. Sparse models by iteratively reweighted feature scaling: A framework for wavelength and sample selection. *J. Chemom.* **2013**, *27*, 50–62. [CrossRef]
26. Filzmoser, P.; Gschwandtner, M.; Todorov, V. Review of sparse methods in regression and classification with application to chemometrics. *J. Chemom.* **2012**, *26*, 42–51. [CrossRef]
27. Irvine, T.N.; Baragar, W. A guide to the chemical classification of the common volcanic rocks. *Can. J. Earth Sci.* **1971**, *8*, 523–548. [CrossRef]
28. Sautter, V.; Toplis, M.J.; Wiens, R.C.; Cousin, A.; Fabre, C.; Gasnault, O.; Maurice, S.; Forni, O.; Lasue, J.; Ollila, A.; et al. In situ evidence for continental crust on early Mars. *Nat. Geosci.* **2015**, *8*, 605–609. [CrossRef]
29. McSween, H.Y.; Taylor, G.J.; Wyatt, M.B. Elemental composition of the Martian crust. *Science* **2009**, *324*, 736–739. [CrossRef]
30. McLennan, S.M.; Anderson, R.B.; Bell, J.F., III; Bridges, J.C.; Calef, F., III; Campbell, J.L.; Clark, B.C.; Clegg, S.; Conrad, P.; Cousin, A.; et al. Elemental Geochemistry of Sedimentary Rocks at Yellowknife Bay, Gale Crater, Mars. *Science* **2014**, *343*, 1244734. [CrossRef]
31. Mangold, N.; Dehouck, E.; Fedo, C.; Forni, O.; Achilles, C.; Bristow, T.; Downs, R.; Frydenvang, J.; Gasnault, O.; L'haridon, J. Chemical alteration of fine-grained sedimentary rocks at Gale crater. *Icarus* **2019**, *321*, 619–631. [CrossRef]
32. Chide, B.; Maurice, S.; Murdoch, N.; Lasue, J.; Bousquet, B.; Jacob, X.; Cousin, A.; Forni, O.; Gasnault, O.; Meslin, P.-Y. Listening to laser sparks: A link between Laser-Induced Breakdown Spectroscopy, acoustic measurements and crater morphology. *Spectrochim. Acta Part B At. Spectrosc.* **2019**, *153*, 50–60. [CrossRef]
33. Rauschenbach, I.; Lazic, V.; Pavlov, S.; Hübers, H.-W.; Jessberger, E. Laser induced breakdown spectroscopy on soils and rocks: Influence of the sample temperature, moisture and roughness. *Spectrochim. Acta Part B At. Spectrosc.* **2008**, *63*, 1205–1215. [CrossRef]
34. Harmon, R.S.; Russo, R.E.; Hark, R.R. Applications of laser-induced breakdown spectroscopy for geochemical and environmental analysis: A comprehensive review. *Spectrochim. Acta Part B At. Spectrosc.* **2013**, *87*, 11–26. [CrossRef]
35. Senesi, G.S. Laser-Induced Breakdown Spectroscopy (LIBS) applied to terrestrial and extraterrestrial analogue geomaterials with emphasis to minerals and rocks. *Earth-Sci. Rev.* **2014**, *139*, 231–267. [CrossRef]